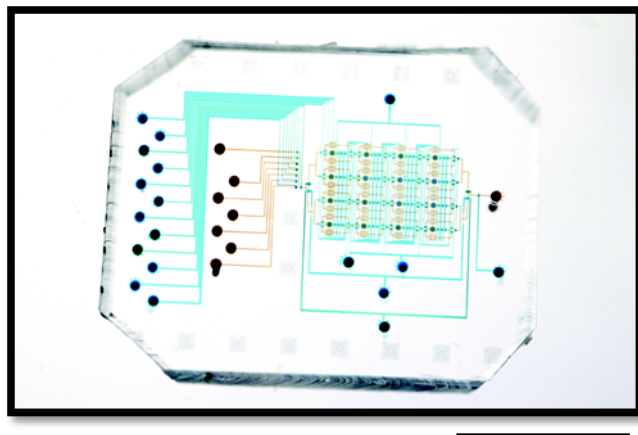


## Supporting Information

# **A Digital-Analog Microfluidic Platform for Patient-Centric Multiplexed Biomarker Diagnostics of Ultra-Low Volume Samples**

*Francesco Piraino<sup>‡</sup>, Francesca Volpetti<sup>‡</sup>, Craig Watson, and Sebastian J. Maerkl\**



**Figure S1. Photograph of the final digital-analog microfluidic device. Control lines and button/membranes (blue) are aligned with flow channels (red). Scale bar 1cm.**

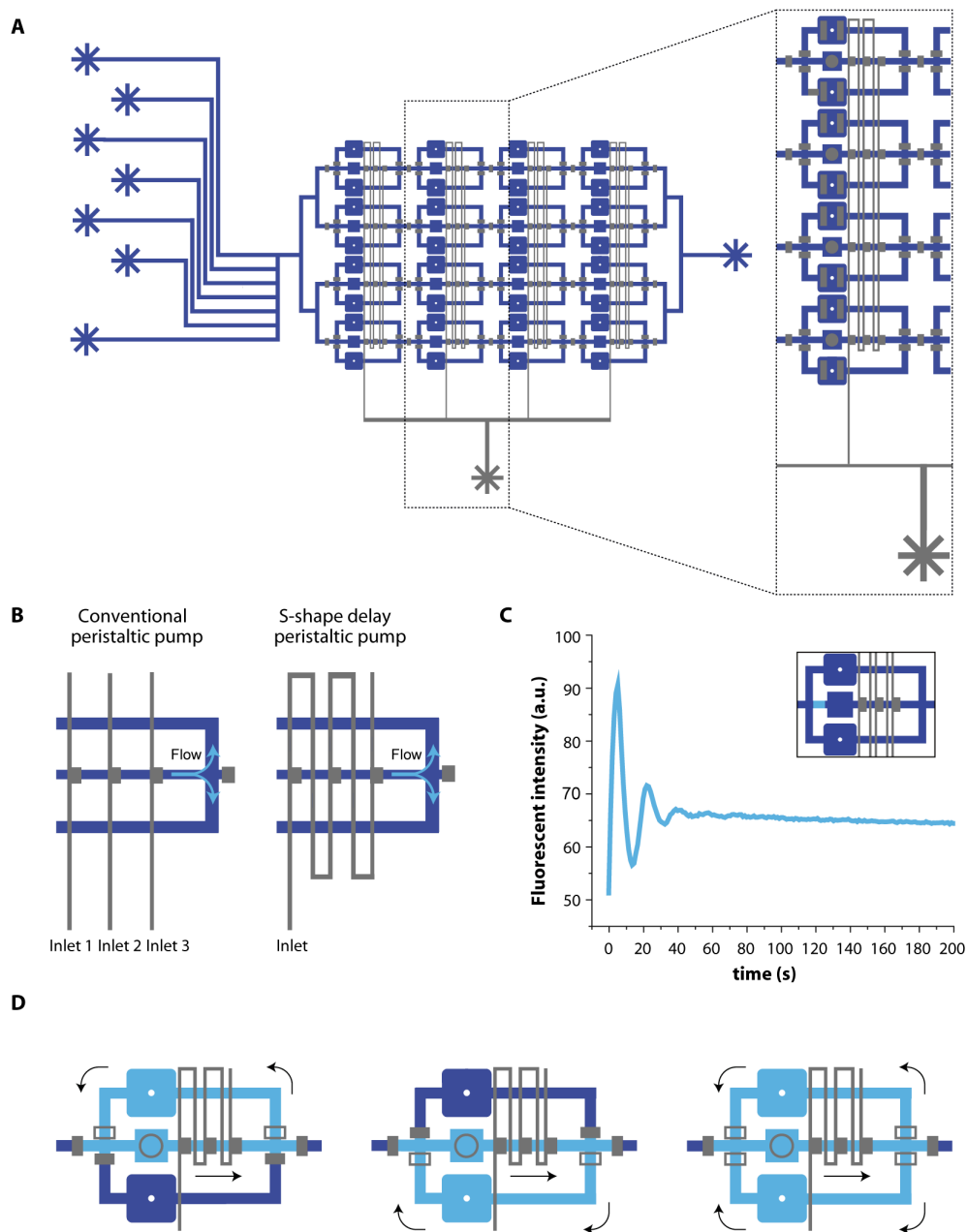


**Figure S2. Serpentine-shape (S-shape) delay peristaltic pump. (A) Schematic of the S-shape delay peristaltic pump used in this study and magnified view of a single column. (B) Schematic illustrations of the difference between a conventional peristaltic pump, in which 3 independent valves are activated in sequence, and the S-shape delay peristaltic pump, in which a single channel is able to perform the mixing. (C) Cy3 labeled solution mixing measurement at a frequency of  $\sim 8.3$  Hz ( $t_{\text{open}} = t_{\text{close}} = 60$  ms) and  $P = 25$  psi. (D) A schematic illustration of the possible flow modes.**



**Figure S3. Activity traces and observed turnover rates of enzymes for the  $\beta$ G assay. (A) Activity traces of enzymes for the  $\beta$ G assay. Turnover rates are determined by linear regression fitting (solid red lines) to the fluorescence trajectories after background subtraction. (B) Histograms of observed turnover rates for individual femtowells. The numbers of wells are plotted *versus* the increase in observed rate. For 0.5, 5, and 25 pM the peaks were fitted with a sum of Gaussians. The values displayed above each peak are the centers of these Gaussians. The inserts show the probability distribution. The black bars represent the experimentally obtained probability distributions calculated from the Gaussian fits. Red data points represent the values obtained from the Poisson distribution  $f(k;\lambda)=\lambda^k e^{-\lambda}/k!$  with the parameter  $\lambda$  equal to the expected number of enzymes per chamber for 0.5, 5, and 25 pM of  $\beta$ G. Blue data points are the values obtained from the Poisson distribution for 12.5 pM of  $\beta$ G. The bin size for all histograms is  $50 \text{ s}^{-1}$ .**

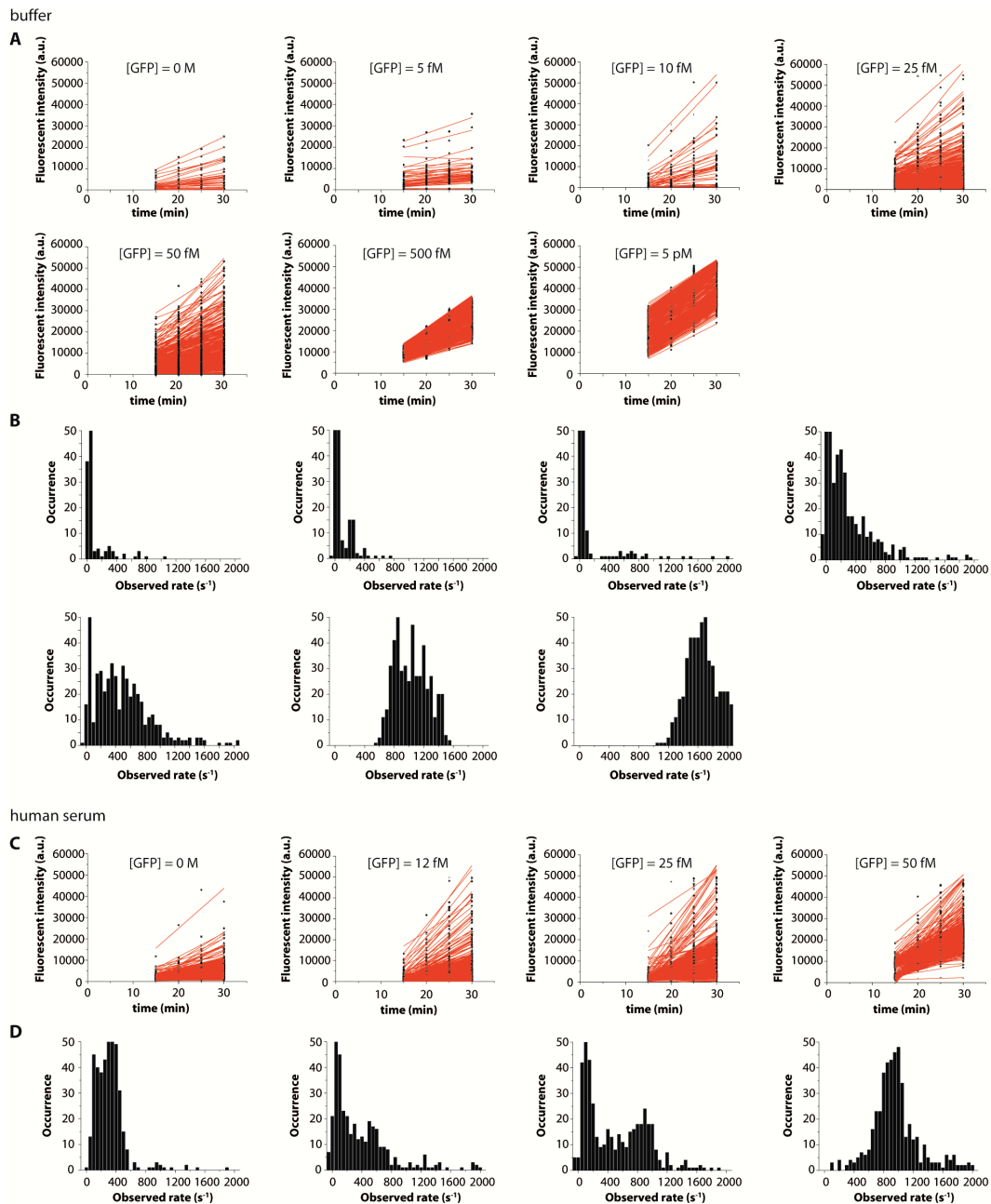


**Figure S4. Activity traces and observed turnover rates of enzymes for the digital-MITOMI immunoassay. (A) Enzyme activity traces for GFP detection in 2% BSA. Turnover rates are determined by linear regression fitting (solid red lines) to the fluorescence trajectories after background subtraction. (B) Histograms of observed turnover rates of individual femtowells. (C) Enzyme activity traces for GFP detection in human serum. (D) Histograms of observed turnover rates. The bin size for all histograms is  $50 s^{-1}$ .**

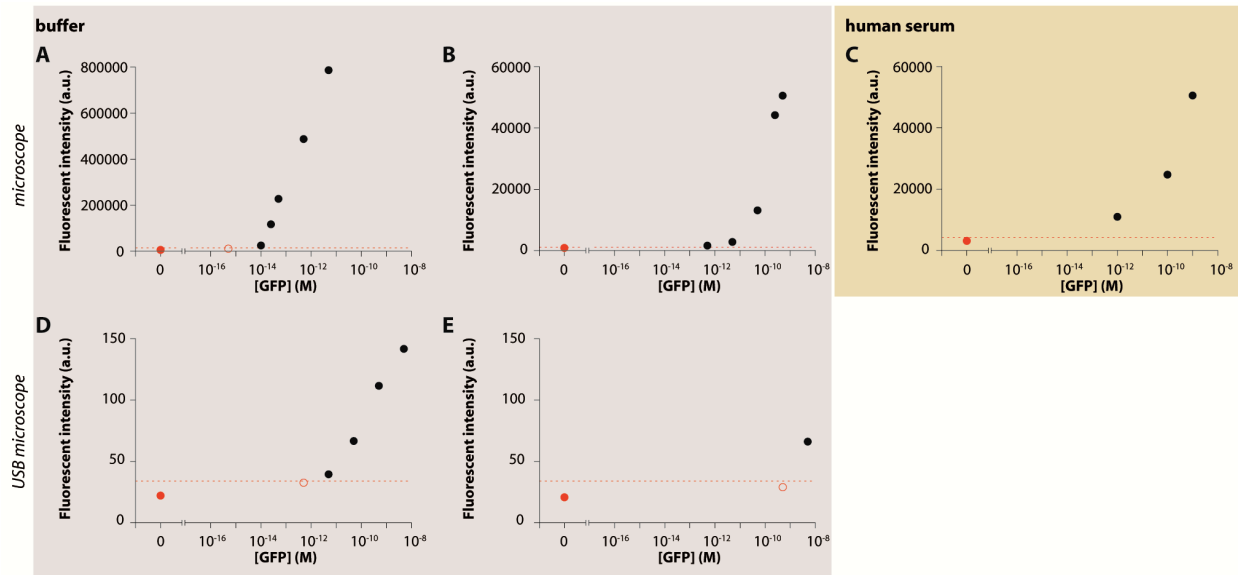


**Figure S5. GFP quantitation. (A-B) Detection of GFP in 2% BSA PBS buffer solution over concentrations ranging from 10 fM to 5 pM. (A) Digital-MITOMI GFP immunoassay. Plotted is the sum of slopes of all femtowells above a background threshold. (B) Analog-MITOMI GFP immunoassay. Plotted is the intensity of Cy3 signal as function of GFP concentration. (C) Digital-MITOMI detection of GFP in human serum over concentrations ranging from 12 fM to 50 fM. Intensity of fluorescein signal is plotted as function of GFP concentration. Data were obtained with a research grade fluorescent microscope. (D-E) Detection of GFP in 2% BSA PBS buffer solution with concentrations ranging from 500 fM to 5 nM. (D) Analog amplification detection of GFP. (E) Analog-MITOMI detection of GFP. Data were obtained with a USB fluorescent microscope. LODs (dashed red lines) were defined as the signal of a negative control sample plus 3 standard deviations.**

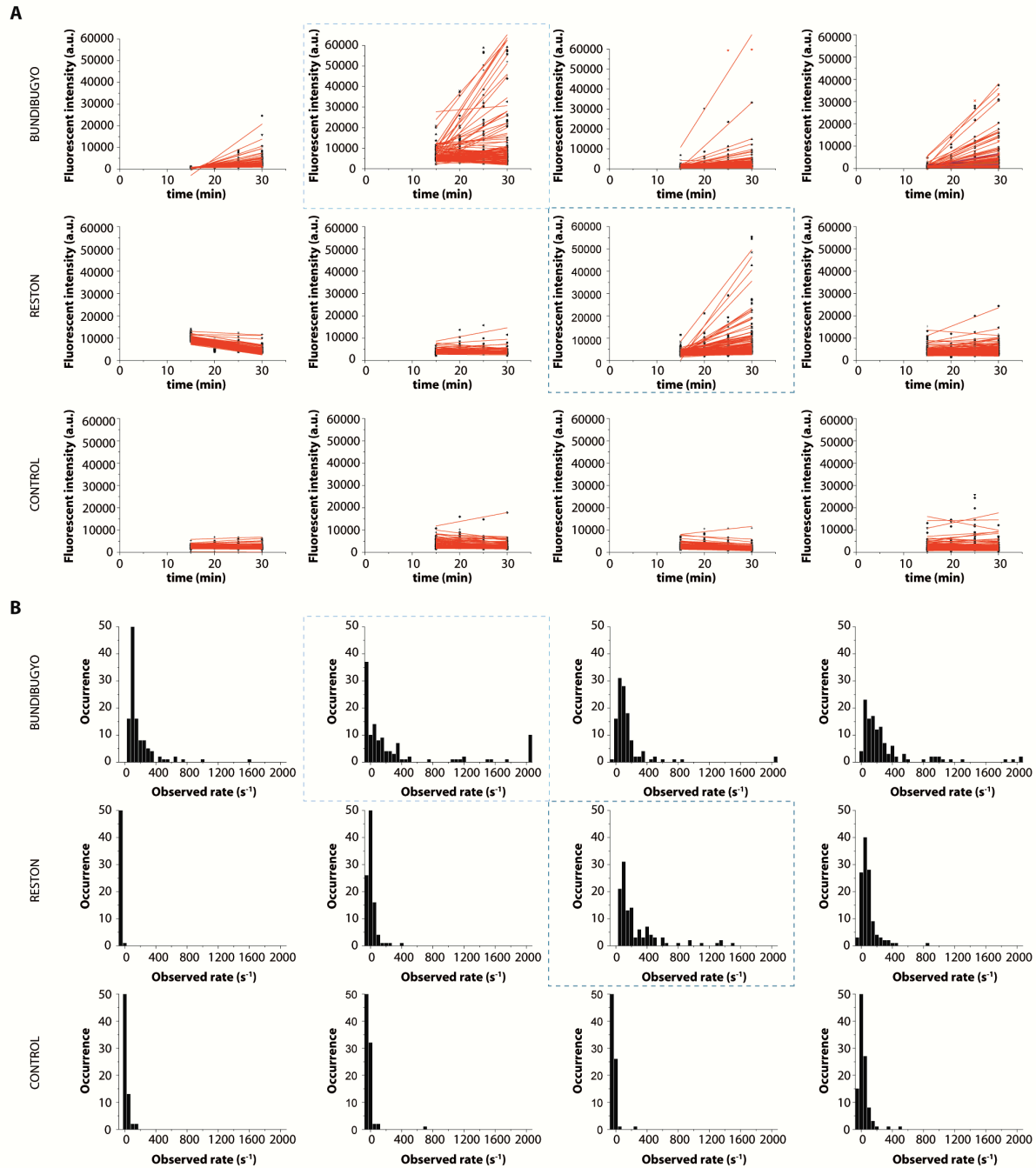


**Figure S6. Activity traces and turnover rates of enzymes for multiplexed digital Ebola diagnostics. (A) Enzyme activity traces for detection of anti-Bundibugyo, anti-Reston and control. Turnover rates are determined by linear regression fitting (solid red lines) to the fluorescence trajectories after background subtraction. (B) Histograms of observed rates of enzymes. Dashed rectangles indicate the position where the positive reaction took place along the channel. The bin size for all histograms is  $50 s^{-1}$ .**

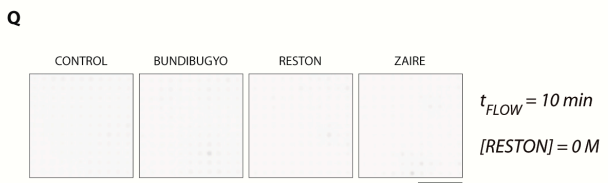
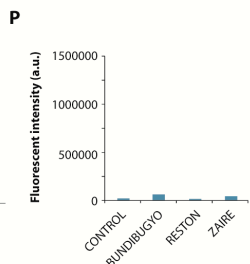
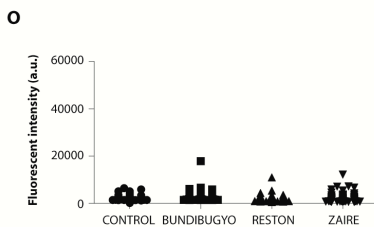
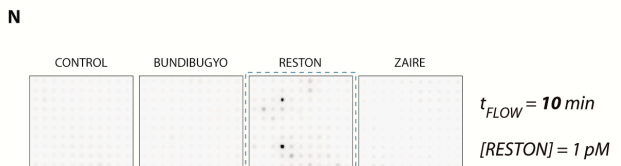
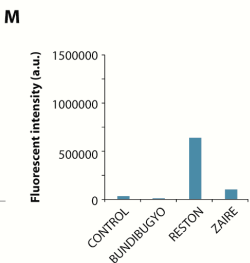
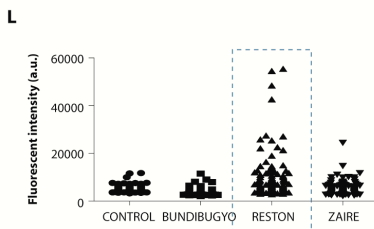
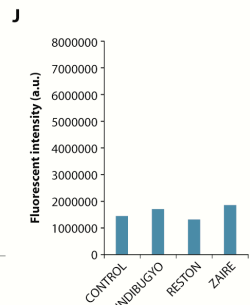
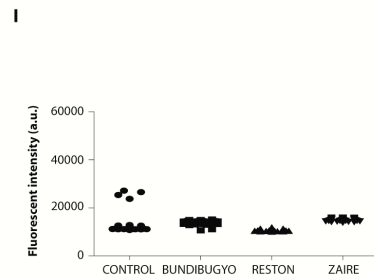
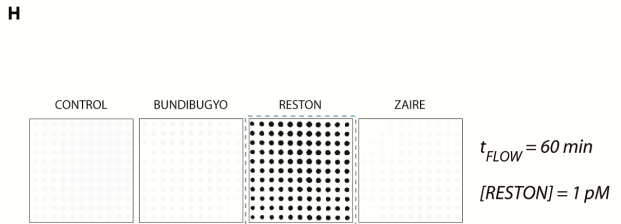
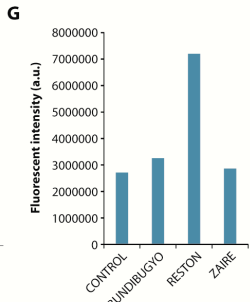
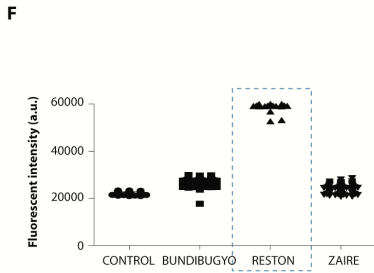
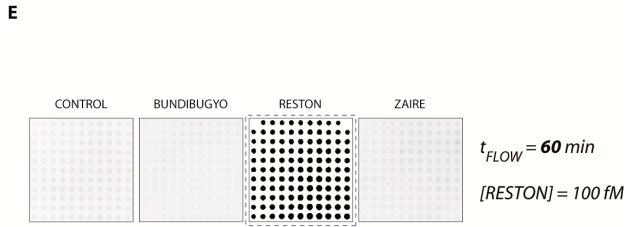
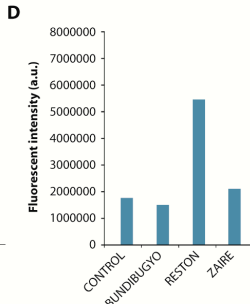
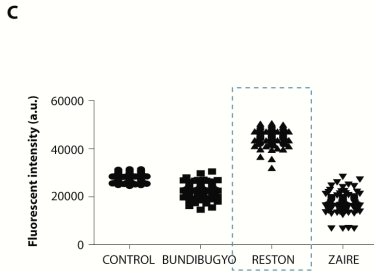
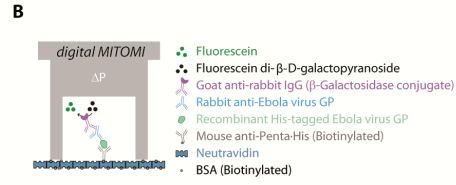
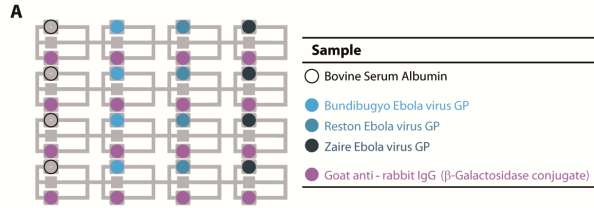


**Figure S7. Multiplexed digital anti-Reston Ebola diagnostics in human serum. (A) Schematic of assay reagents allocation on the device. (B) Schematic of the assay for digital-MITOMI anti-Ebola virus detection. (C-E) 100 fM (flowed for 60 min) anti-Reston Ebola GP IgG antibody, (F-H) 1 pM (flowed for 60 min) anti-Reston Ebola GP IgG antibody, (I-K) 0 M (flowed for 60 min) anti-Reston Ebola GP IgG antibody, (L-N) 1 pM (flowed for 10 min) anti-Reston Ebola GP IgG antibody, and (O-Q) 0 M (flowed for 10 min) anti-Reston Ebola GP IgG antibody. Shown are the signals obtained from individual femtowells (C,F,I), the sum of the signal in positive femtowells (D,G,J), and examples of a digital-MITOMI button for each sample (E,H,K). All measurements were performed in human serum.**

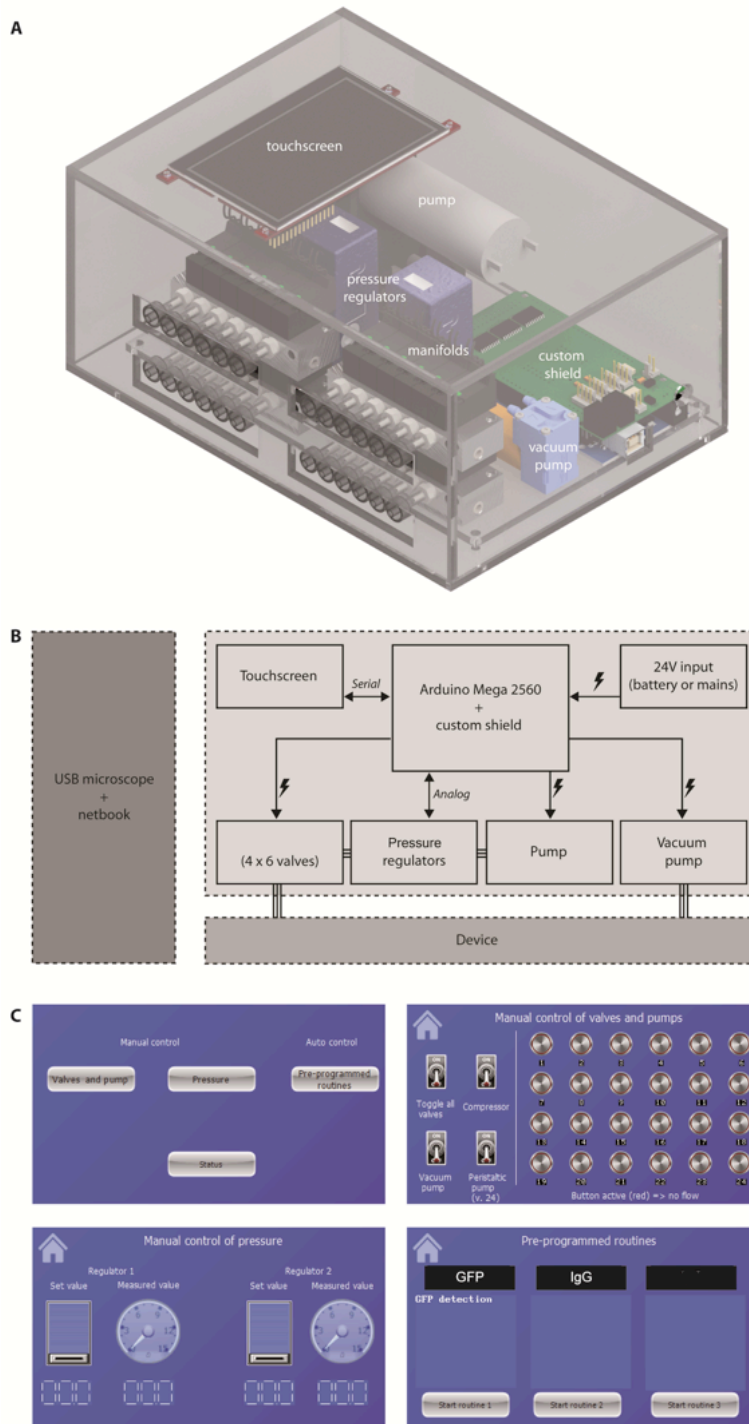


**Figure S8 3D rendering, block diagram and overview of the graphical user interface of the MSC. (A) 3D rendering of the MSC showing how the different components were arranged. (B) The system consists of an Arduino Mega 2560 coupled with an electronic PCB (custom shield), a touchscreen, a battery, a pneumatic system (manifold, pressure regulators, pumps), and an imaging/analysis module (USB microscope + netbook). (C) Several possible control modes are available to the user: (1) manual control of the compressor, vacuum pump, peristaltic pump and individual valves; (2) manual control of pressure; (3) pre-programmed routines for GFP and IgG detection.**

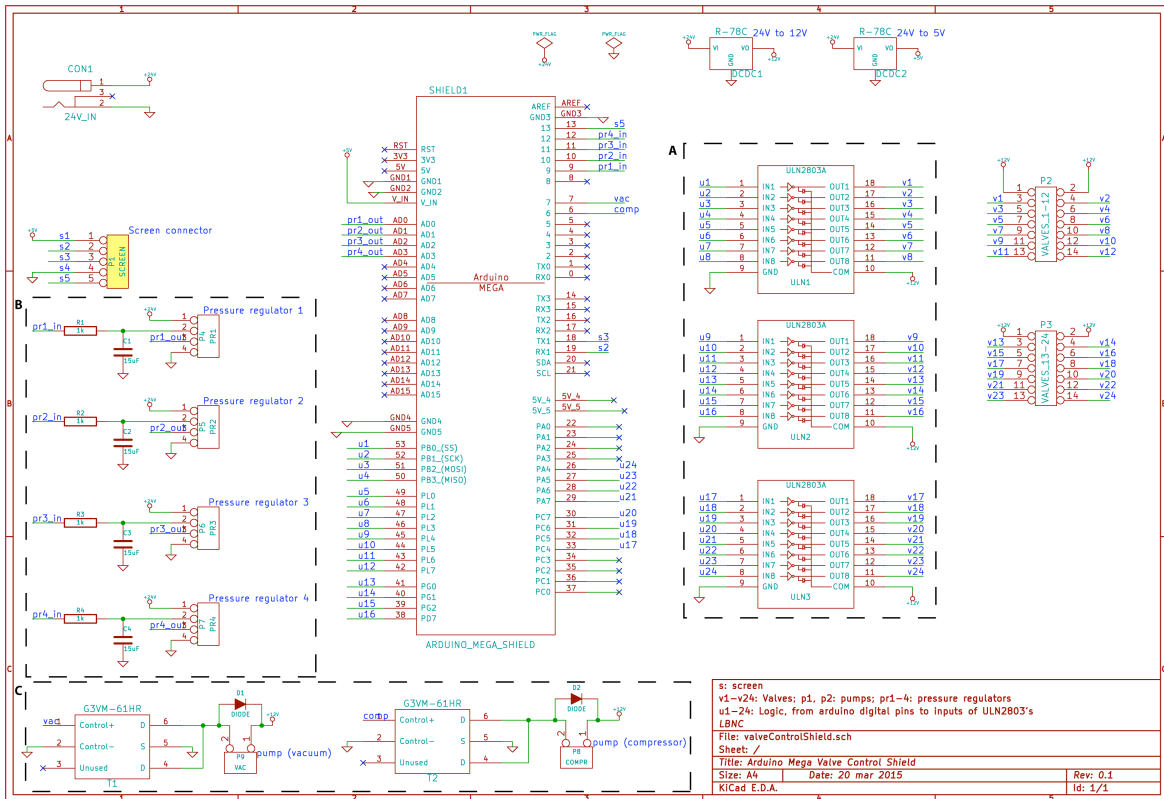


**Figure S9. Circuit diagram of the PCB. (A) ULN2803 transistor array. One digital pin of the Arduino is connected to each IN pin of the ULN. Applying +5 V to the IN, allows current to pass from the corresponding OUT pin to the ground and thus through the load that is connected to the OUT pin - in this case, a solenoid valve. Three ULN2803's are used to drive the 24 valves of the MSC. (B) Pressure regulators. A low-pass filter converts the PWM signal from the Arduino ("pr1\_in") to an analog voltage that can be read by the regulator on pin 2. Pin 3 is the output voltage indicating the current pressure, and goes to the Arduino pin labeled "pr1\_out". (C) Transistors for the pumps. Applying +5 V to the control + pin allows current to pass through the pump and from the drain to the source. The diode wired in parallel with the pump protects the circuit from voltage spikes occurring when the pump is switched off.**

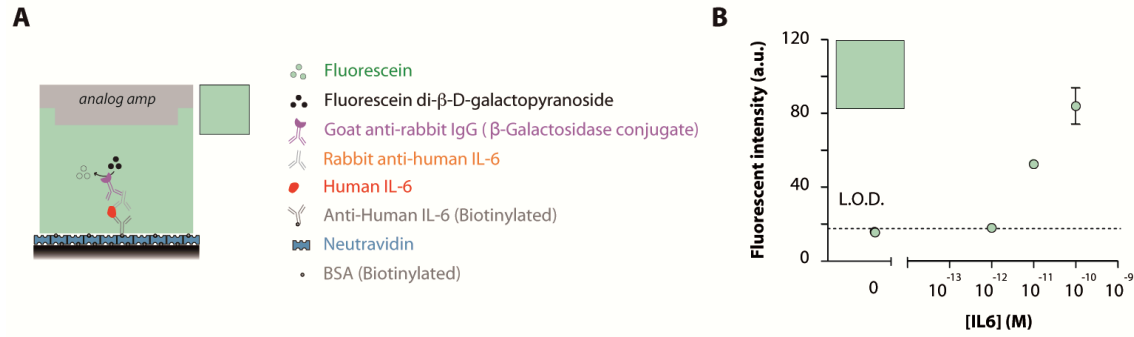
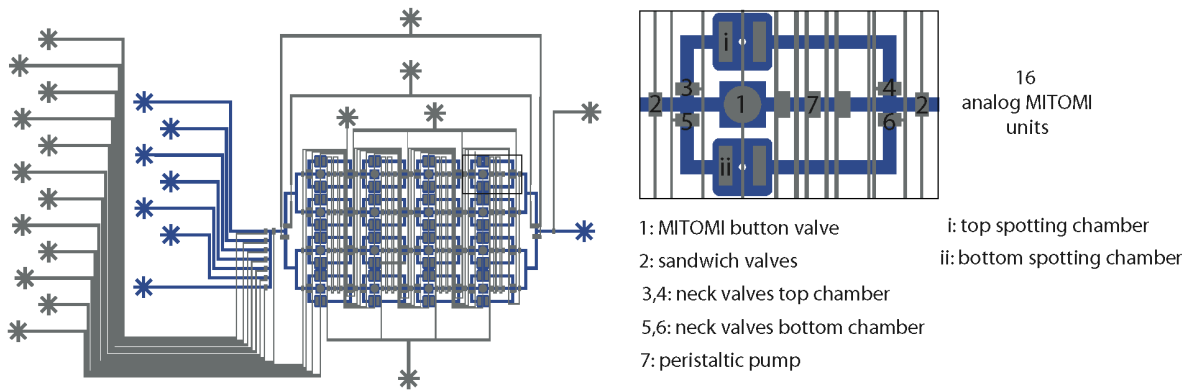
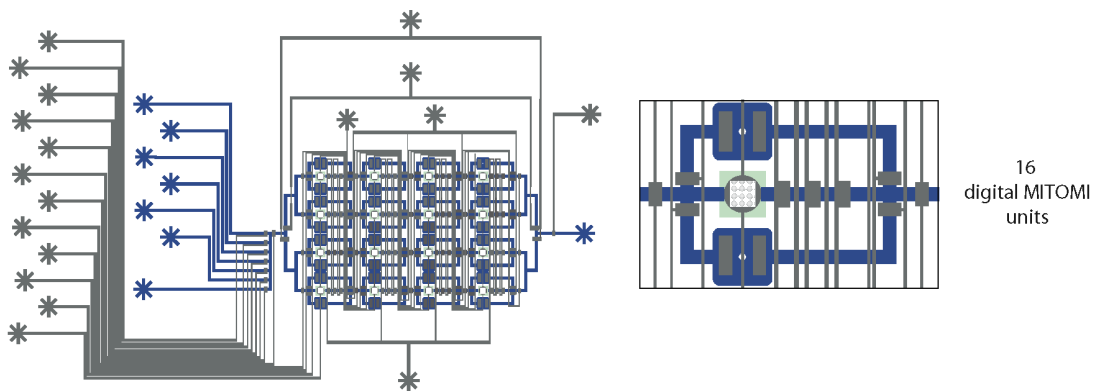


**Figure S10. (A) Schematic of the IL-6 sandwich assays performed on the microfluidic device and detected with analog amplification. (B) Detection of IL-6 in human serum with concentrations ranging from 100 pM to 1 pM. Data were obtained with a fluorescence USB microscope. LODs were determined from the signal of a negative control plus 3 standard deviations.**

**A** Analog MITOMI



**B** Digital MITOMI



**C** Digital-Analog MITOMI

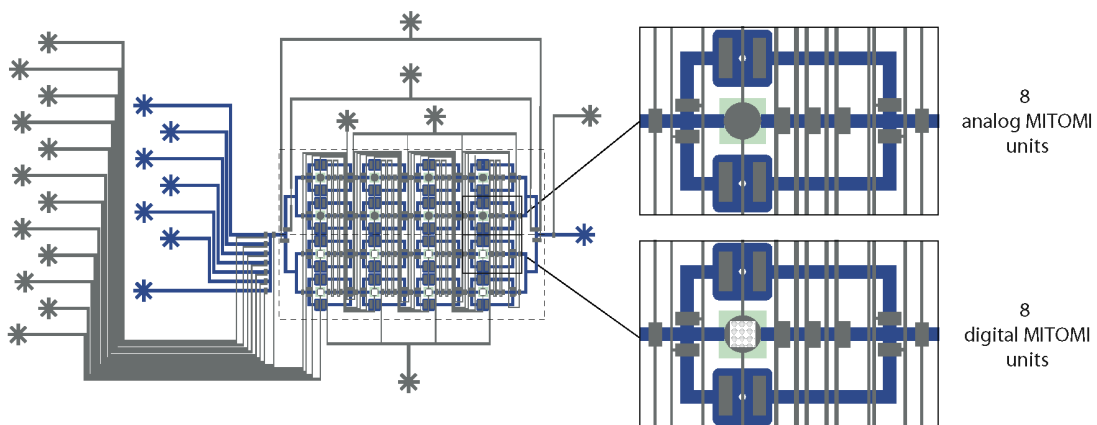


**Figure S11. Microfabricated diagnostic devices used in this study. (A) Design schematic of the analog MITOMI microfluidic device showing flow (blue) and control (gray) layers. The device has four rows; each row contains four unit cells for a total of 16 analog assay units. Each assay unit (inset) contains: a MITOMI button valve (1), a sandwich valve (2), two neck valves (3, 4) for the top chamber (*i*) and two (5, 6) for the bottom one (*ii*), and a peristaltic pump (8). (B) Digital MITOMI device. (C) Digital-analog hybrid MITOMI device, with 8 digital and 8 analog units.**

**Table S1. Comparison of the  $\mu$ FDS with the microfluidic platform technologies for biomarker diagnostics.**

	Digital	Analog	Limit Of Detection	Dynamic Range [orders of magnitude]	Sample volume [ $\mu$ l]	Dilution required	Multiplexing [units]
This study	✓	✓	~330 fg/ml	5	5	-	16
Wu <i>et al.</i> <sup>1</sup>	✓	x	1 fg/ml - 0.09 pg/ml	>4	100	1:4	10
Rissin <i>et al.</i> <sup>2</sup>	✓	x	~6-10 fg/ml	4	100	1:4	2
Rissin <i>et al.</i> <sup>3</sup>	✓	x	3 fg/ml	4	100	-	4
Inci <i>et al.</i> <sup>4</sup>	x	✓	400 fg/ml	8	≤100	1:10	-
Fan <i>et al.</i> <sup>5</sup>	x	✓	17.5 pg/ml	4	10	1:10	12
Kadimisetty <i>et al.</i> <sup>6</sup>	x	✓	10-100 fg/ml	5	5-10	1:30-500	6
Krause <i>et al.</i> <sup>7</sup>	x	✓	10-40 fg/ml	3	5	1:30	4

**Table S2. Cost table of  $\mu$ Fluidic Diagnostic System.**

<b>Part description</b>	<b>Vendor</b>	<b>Part no.</b>	<b>Unit price (USD)</b>	<b>Quantity</b>	<b>Total (USD)</b>
6 valve manifold	Pneumadyne	S14-2936	174.35	4	697.40
Vacuum pump	Parker	E163-11-120	68.57	1	68.57
Air pump	Amazon	TM40-A	66.35	1	66.35
<u>Electronic P controllers</u>	<u>Parker</u>	<u>990-005103-015</u>	<u>185.71</u>	<u>2</u>	<u>371.41</u>
Arduino Mega 2560	Amazon	642819	37.76	1	37.76
Printed Circuit Board	Euro Circuits	Custom	65.09	1	65.09
Locking male header, 2-pin	Digi-Key	A1921-ND	0.12	2	0.24
Locking male header, 4-pin	Digi-Key	A19431-ND	0.18	4	0.72
Header pins	Digi-Key	S1012E-36-ND	1.61	2	3.22
Capacitors	Digi-Key	399-10449-1-ND	0.39	4	1.55
Diodes	Digi-Key	641-1017-1-ND	0.28	2	0.56
Power jack 2.1mm	Digi-Key	CP-002A-ND	0.96	1	0.96
Resistors	Digi-Key	P1.0KJCT-ND	0.10	4	0.40
DC/DC converter 5V out	Digi-Key	945-1395-5-ND	9.03	1	9.03
DC/DC converter 12V/3A out	Digi-Key	945-1729-5-ND	24.54	1	24.54
Transistor arrays (ULN2803)	Digi-Key	296-15777-2-ND	0.99	3	2.97
Transistors (for compressors)	Digi-Key	Z3099-ND	12.67	2	25.34
<u>4.3" LCD module w/ Res Touch</u>	<u>Mouser</u>	<u>uLCD-43PT</u>	<u>150.18</u>	<u>1</u>	<u>150.18</u>
Rechargeable Battery	BixPower	Bat-MP100-24V	139.95	1	139.95
					-----
<b>Microfluidic Control System</b>					<b>1666.24</b>
USB microscope	VWR International	AM4113T-FBW	827.84	1	827.84
Netbook	Amazon	n/a	134.31	1	134.31

**Table S3. Liquid handling sequence for the digital-MITOMI immunoassay.**

	<b>Reagent</b>	<b>time (min)</b>
1	BSA (Biotinylated)	10
2	PBS-tween	5
3	Neutravidin	10
4	PBS-tween	5
5	BSA (Biotinylated)	10
6	PBS-tween	5
7	Goat anti-GFP (Biotinylated)	10
8	PBS-tween	5
9	GFP	10
10	PBS-tween	5
11	Mouse anti-Penta His (Alexa Fluor 555 conjugate)	8
12	PBS-tween	5
13	Goat anti-mouse IgG ( $\beta$ G conjugate)	10
14	PBS-tween	5
15	FDG	4

**Table S4. Liquid handling sequence for the analog-amp IL-6 MITOMI immunoassay.**

	<b>Reagent</b>	<b>time (min)</b>
1	BSA (Biotinylated)	10
2	PBS-tween	5
3	Neutravidin	10
4	PBS-tween	5
5	BSA (Biotinylated)	10
6	PBS-tween	5
7	Anti-Human IL6 (Biotinylated)	10
8	PBS-tween	5
9	Human IL6	10
10	PBS-tween	5
11	Rabbit anti-Human IL6	8
12	PBS-tween	5
13	Goat anti-rabbit IgG ( $\beta$ G conjugate)	10
14	PBS-tween	5
15	FDG	4

**Table S5. Liquid handling sequence for multiplexed Ebola diagnostics.**

	<b>Reagent</b>	<b>time (min)</b>
1	BSA (Biotinylated)	10
2	PBS-tween	5
3	Neutravidin	10
4	PBS-tween	5
5	BSA (Biotinylated)	10
6	PBS-tween	5
7	Mouse anti-Penta His (Biotinylated)	10
8	PBS-tween	5
9	Pumping GP	10
10	PBS-tween	5
11	Sample	8
12	PBS-tween	5
13	Pumping secondary antibody	10
14	PBS-tween	5
15	FDG	4

## SUPPLEMENTARY REFERENCES

1. Wu, D.; Milutinovic, M. D.; Walt, D. R. Single Molecule Array (Simoa) Assay with Optimal Antibody Pairs for Cytokine Detection in Human Serum Samples. *Analyst* **2015**, *140*, 6277-82.
2. Rissin, D. M.; Kan, C. W.; Campbell, T. G.; Howes, S. C.; Fournier, D. R.; Song, L.; Piech, T.; Patel, P. P.; Chang, L.; Rivnak, A. J.; Ferrell, E. P.; Randall, J. D.; Provuncher, G. K.; Walt, D. R.; Duffy, D. C. Single-Molecule Enzyme-Linked Immunosorbent Assay Detects Serum Proteins at Subfemtomolar Concentrations. *Nat. Biotechnol.* **2010**, *28*, 595-599.
3. Rissin, D. M.; Kan, C. W.; Song, L.; Rivnak, A. J.; Fishburn, M. W.; Shao, Q.; Piech, T.; Ferrell, E. P.; Meyer, R. E.; Campbell, T. G.; Fournier, D. R.; Duffy, D. C. Multiplexed Single Molecule Immunoassays. *Lab Chip* **2013**, *13*, 2902-11.
4. Inci, F.; Filippini, C.; Baday, M.; Ozen, M. O.; Calamak, S.; Durmus, N. G.; Wang, S.; Hanhauser, E.; Hobbs, K. S.; Juillard, F.; Kuang, P. P.; Vetter, M. L.; Carocci, M.; Yamamoto, H. S.; Takagi, Y.; Yildiz, U. H.; Akin, D.; Wesemann, D. R.; Singhal, A.; Yang, P. L. *et al.* Multitarget, Quantitative Nanoplasmonic Electrical Field-Enhanced Resonating Device (NE<sup>2</sup>RD) for Diagnostics. *Proc. Natl. Acad. Sci. U.S.A.* **2015**, *112*, E4354-63.
5. Fan, R.; Vermesh, O.; Srivastava, A.; Yen, B. K.; Qin, L.; Ahmad, H.; Kwong, G. A.; Liu, C. C.; Gould, J.; Hood, L.; Heath, J. R. Integrated Barcode Chips for Rapid, Multiplexed Analysis of Proteins in Microliter Quantities of Blood. *Nat. Biotechnol.* **2008**, *26*, 1373-1378.
6. Kadimisetty, K; Malla, S.; Sardesai, N. P.; Joshi, A. A.; Faria, R. C.; Lee, N. H.; Rusling, J. F. Automated Multiplexed ECL Immunoarrays for Cancer Biomarker Proteins. *Anal. Chem.* **2015**, *87*, 4472-4478.
7. Krause, C. E.; Otieno, B. A.; Latus, A.; Faria, R. C.; Patel, V.; Gutkind, J. S.; Rusling, J. F. Rapid Microfluidic Immunoassays of Cancer Biomarker Proteins Using Disposable Inkjet-Printed Gold Nanoparticle Arrays. *ChemistryOpen* **2013**, *2*, 141-145.